AGU ADVANCING EARTH AND SPACE SCIENCE

Geophysical Research Letters®

RESEARCH LETTER
10.1029/2021GL096082

On the Controlling Factors for Globally Extreme Humid Heat

Colin Raymond[1], Tom Matthews[2], Radley M. Horton[3,4], Erich M. Fischer[5], Stephan Fueglistaler[6], Catherine Ivanovich[3], Laura Suarez-Gutierrez[7], and Yi Zhang[6]

[1]Jet Propulsion Laboratory/California Institute of Technology, Pasadena, CA, USA, [2]Geography, King's College London, London, UK, [3]Earth and Environmental Sciences, Columbia University, New York, NY, USA, [4]Lamont-Doherty Earth Observatory, Columbia University, Palisades, NY, USA, [5]Environmental Systems Science, ETH Zurich, Zurich, Switzerland, [6]Program in Atmospheric and Oceanic Sciences, Princeton University, Princeton, NJ, USA, [7]Max Planck Institute for Meteorology, Hamburg, Germany

Abstract Humid heat presents a major societal challenge through its impacts on human health, energy demand, and economic productivity, underlined by the projected emergence of conditions beyond human tolerance. However, systematic assessment of what drives the most extreme humid heat worldwide has been lacking. Here, we investigate factors determining the location and magnitude of humid-heat extremes, framing our analysis around the four regions with the highest values: the southern Persian Gulf, north-central Pakistan, eastern South Asia, and the western Amazon. We find that strong boundary-layer moisture fluxes, together with stability that inhibits moist convection, explain well the timing and location of near-surface humid-heat extremes. These favorable conditions are achieved through regionally distinct factors, including shallow sea breezes in the Persian Gulf and large-scale subsidence in eastern South Asia. Our results demonstrate some of the principal controls on the most intense humid heat, both globally and for particular regions and heat events.

Plain Language Summary Combinations of high temperatures and high humidity are a primary threat of climate change because they can be not only uncomfortable but deadly, and are growing rapidly in frequency and intensity. In this study, we present a general theory for where the most extreme such events occur and describe the precise meteorological conditions that favor them. We are therefore able to state with new confidence the reasons why extreme humid heat events take place where they do, and why. Our results also highlight the regional distinctions in the factors (such as winds or ocean temperatures) that contribute to these events, increasing the strength of the evidence that some regions are much more sensitive to certain factors than others—information that can be used to guide better forecasts as well as climate-change projections.

Key Points:

- A systematic assessment of humid-heat hotspots reveals the dual importance of vertical stability and low-level moisture sources
- These two conditions are achieved through markedly different meteorological processes and in markedly different geographical contexts
- Understanding the most extreme humid heat requires applying global principles to detailed regional analyses across space and time scales

Supporting Information:

Supporting Information may be found in the online version of this article.

Correspondence to:

C. Raymond,
colin.raymond@jpl.nasa.gov

Citation:

Raymond, C., Matthews, T., Horton, R. M., Fischer, E. M., Fueglistaler, S., Ivanovich, C., et al. (2021). On the controlling factors for globally extreme humid heat. *Geophysical Research Letters*, *48*, e2021GL096082. https://doi.org/10.1029/2021GL096082

Received 8 SEP 2021
Accepted 6 NOV 2021

Author Contributions:

Conceptualization: Tom Matthews, Radley M. Horton
Validation: Tom Matthews
Writing – review & editing: Tom Matthews, Radley M. Horton, Erich M. Fischer, Stephan Fueglistaler, Catherine Ivanovich, Laura Suarez-Gutierrez, Yi Zhang

1. Introduction

Extreme humid heat—the combination of high temperatures and specific humidity—is rapidly intensifying globally and poses a threat to societies in multiple climate zones through its impacts on human health, energy demand, and economic productivity (Buzan & Huber, 2020; Chen et al., 2020; Dunne et al., 2013; Li et al., 2020; Mora et al., 2017; Raymond et al., 2020). It is only recently that climate studies have treated moisture as an important dimension for understanding location and timing of impactful regional heat extremes, both presently and for future climate change (Buzan & Huber, 2020; Coffel et al., 2019; Fischer & Knutti, 2013; Mishra et al., 2020). Under continued warming, hundreds of millions of people are at risk of exposure to humid heat beyond physiological limits (Hanna & Tait, 2015; Im et al., 2017; Pal & Eltahir, 2016). Although humid heat reaches its highest values in the subtropics (Raymond et al., 2020; Zhang et al., 2021), no studies to date have systematically investigated why. Additionally, the meteorological conditions conducive to extreme humid heat vary considerably among regions, as revealed by studies of the United States, Middle East, and portions of Asia (Freychet et al., 2020; Im et al., 2017, 2018; Monteiro & Caballero, 2019; Pal & Eltahir, 2016; Raymond et al., 2017). As a result of this complexity, a global framework explaining the locations and magnitudes of the most extreme humid heat, theoretically or empirically, has remained elusive.

Our investigation is designed to advance toward this goal, building on knowledge of mechanisms operating at regional scales—such as monsoonal moisture advection and surface latent-heat fluxes (Monteiro & Caballero, 2019; Xue & Eltahir, 2015)—and on patterns identified in global surveys (Buzan & Huber, 2020; Matthews, 2018; Raymond et al., 2020). By framing our study around the analysis of processes common to "hotspot" regions (those with the highest observed humid heat), we aim to unite existing region-specific studies in a global

process-based framework. Achieving a clearer understanding of its geographic and meteorological characteristics could aid in improving projections and tailoring adaptation and mitigation efforts for this major climate hazard.

To measure humid heat, we use moist enthalpy [ME], defined as the sum of latent-heat and sensible-heat content. ME relates closely to empirical humid-heat metrics (e.g., Matthews, 2018) with serious health impacts (Hanna & Tait, 2015; Kenney et al., 2004). In particular, ME exhibits a nearly one-to-one relationship with wet-bulb temperature (Eltahir & Pal, 1996; Figure S1 in Supporting Information S1), used to characterize thermal tolerance (Im et al., 2018; Pal & Eltahir, 2016; Sherwood & Huber, 2010). ME also enables clear separation of the temperature (sensible) and moisture (latent) contributions to heat stress, which we exploit to help understand the physical processes driving extremes. With the addition of a geopotential term, ME becomes moist static energy (MSE), which is conserved for moist-adiabatic vertical motion. Consistent with previous studies, we use MSE to help understand the role of static (vertical) stability (Bui et al., 2016; Zhang & Fueglistaler, 2020).

We first survey global patterns of extreme ME; then examine processes in four hotspot regions; and finally consider how their commonalities inform a more fundamental understanding of where humid-heat hotspots occur and why.

2. Methods

Our primary dataset is ERA5 reanalysis (Hersbach et al., 2020) over 1979–2018 at a slightly reduced resolution (3-hourly, 0.25° × 0.25°). We use monthly sea-surface temperatures (SSTs) from NOAA OISST (Reynolds et al., 2002), and daily precipitation from CHIRPS2.0 (Funk et al., 2015) to avoid ERA5's Middle Eastern summer precipitation bias (Fallah et al., 2020).

2.1. Calculation of Moist Enthalpy and Moist Static Energy

We calculate ME and MSE from air temperature and specific humidity according to the following equations (Huang, 2018; Matthews, 2018), at the 2-m level and on selected model-native levels throughout the troposphere:

$$e = \frac{\exp\left(34.494 - \frac{4924.99}{T_d - 36.05}\right)}{\left(T_d - 168.15\right)^{1.57}}, T_d > 273.15; e = \frac{\exp\left(43.494 - \frac{6545.8}{T_d + 4.85}\right)}{\left(T_d + 594.85\right)^2}, T_d <= 273.15, \quad (1)$$

for vapor pressure e in Pa, with dew point temperature T_d in K

$$r = 0.62197 * \frac{e}{p - e} \quad (2)$$

for mixing ratio r (unitless), with surface pressure p in Pa

$$c_p = 1005.7 * \left(1 - r\right) + 1850 * r * \left(1 - r\right) \quad (3)$$

for specific heat of moist air c_p in J/kg/K

$$Q_h = c_p * T \quad (4)$$

for sensible heat Q_h in J/kg, with dry-bulb temperature T in K

$$q = \frac{r}{1 + r} \quad (5)$$

for specific humidity q in kg/kg

$$L_v = 1.918 * 10^6 * \left(\frac{T}{T - 33.91}\right)^2 \quad (6)$$

for latent heat of vaporization L_v in J/kg, with T in K

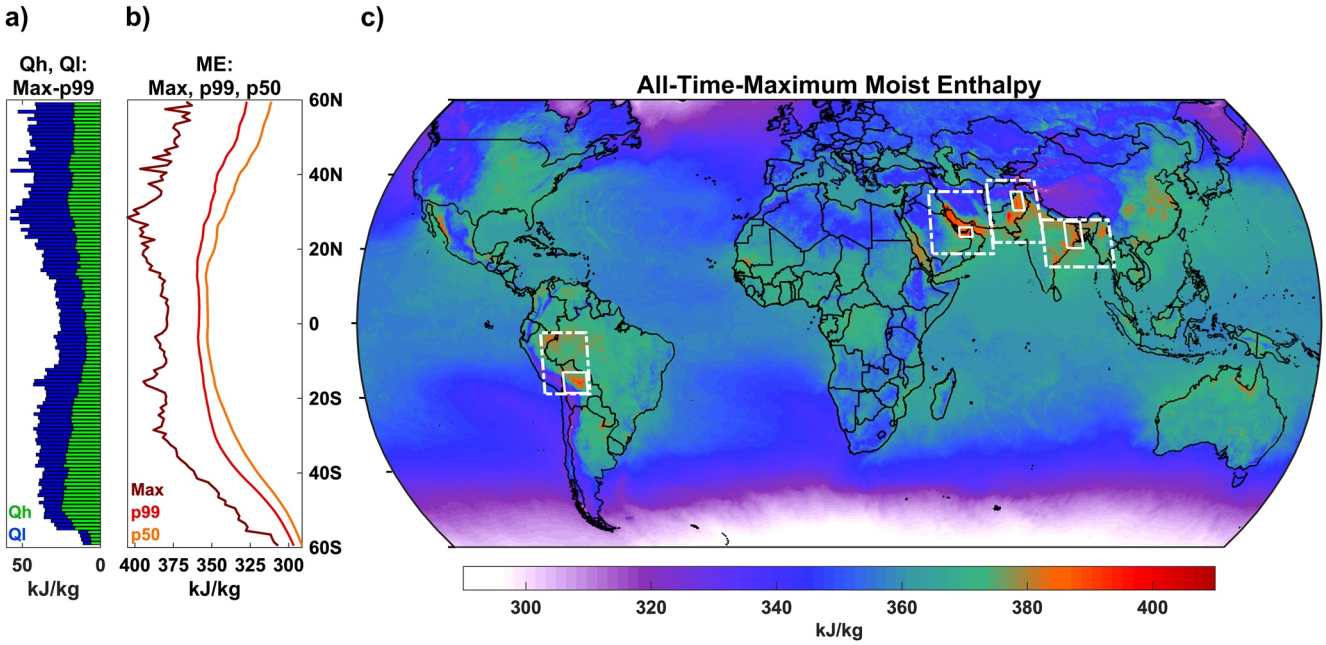

Figure 1. Global extreme values of near-surface moist enthalpy. (a) Difference between all-time maximum and 99th percentile of ME at each latitude from 60ºS to 60ºN, decomposed into sensible-heat (Qh) and latent-heat (Ql) components. (b) All-time maximum and 99th and 50th percentiles of ME at each latitude. (c) All-time maximum ME at each grid cell, with hotspot regions delineated by dash-dot outlines and their subregions by solid outlines.

$$Q_l = L_v * q \tag{7}$$

for latent heat Q_l in J/kg

$$ME = \left(Q_h + Q_l\right)/1000 \tag{8a}$$

for moist enthalpy ME in kJ/kg

$$MSE = \left(Q_h + Q_l + gz\right)/1000 \tag{8b}$$

for moist static energy MSE in kJ/kg, with gravitational acceleration g in m/s^2 and geopotential height z in m

ME contains the two terms relevant to heat stress, and so is used for discussing humid heat at the 2-m level; MSE is used otherwise.

2.2. Definitions of Humid-Heat Extremes and Hotspot Regions

To understand high-end global values and the processes influencing them, we focus on four hotspot regions: the southern Persian (Arabian) Gulf, the Indus Valley of Pakistan, eastern South Asia, and the southern portion of the western Amazon basin (Figure 1). These regions contain the largest number of grid cells exceeding the 99th percentile of the global distribution of all-time grid cell maxima ("global 99th percentile"; Figure S2 in Supporting Information S1), and they represent a range of climate regimes, encompassing coastal and continental; tropical and subtropical; and monsoonal and desert. Regions are defined to include all adjacent grid cells with similar geographic influences, making them of unequal size. To ensure that within each region our results more precisely reflect areas with similar meteorology, we further restrict regional-mean calculations to specific subregions (Figure 1c).

Consistent with our intent to examine the highest global values, we define ME extremes as days when daily-maximum ME at a grid cell exceeds the global 99th percentile. Regional extreme days are defined by constructing a ranking of days according to the count of extreme-ME grid cells, excluding days where this is zero, and then

taking the top decile of days. Applying these definitions yields sample sizes of $n = 163$ days for the Persian Gulf; $n = 109$ for Pakistan; $n = 56$ for eastern South Asia; and $n = 49$ for the western Amazon. Accordingly, results for the latter two regions have the greatest uncertainty.

2.3. Humid-Heat Analysis

In computing composite time series surrounding extreme-ME days, we successively include days before and after only if the daily-maximum ME falls below the global 99th percentile. This approach is intended to prioritize processes that lead to ME extremes, rather than those that sustain it for multiple days consecutively.

To facilitate spatial comparisons and accurately assess anomalous conditions associated with ME extremes, we define each grid cell's warm season as the climatological 90 days per year with the highest ME. These warm seasons are used in calculating grid cell percentiles; all-time maxima, although generally occurring during these seasons, are not restricted to them.

3. Results

We find that the globally highest ME occurs in the subtropics, peaking between 25°N and 30°N (Figure 1b). The 99th and 50th ME percentiles, in contrast, peak in the Northern Hemisphere outer tropics but are high throughout the tropics (Willett & Sherwood, 2012). Hemispheric asymmetry is especially pronounced for all-time-maxima ME, due largely to the latent-heat contribution, which reaches higher anomaly maxima in the Northern Hemisphere subtropics and lower mid-latitudes than at the same Southern Hemisphere latitudes (Figure 1a; Lutsko, 2021). Conversely, the lack of globally extreme ME in the tropics is reflected in the small difference between the all-time maximum and 99th percentile, consistent with fundamental dynamical limits on tropical heat anomalies (Zhang et al., 2021). Within latitude bands, ME extremes are highly concentrated geographically (Figure 1c), as regional studies have highlighted (Im et al., 2017; Pal & Eltahir, 2016; Raymond et al., 2020; Sherwood & Huber, 2010). For example, the Sahara Desert and northern Pakistan lie at 30°N, yet their ME maxima differ substantially (by ~50 kJ/kg). Temperature limitations of marine environments result in lower extreme-ME values over oceans, except for hot subtropical seas such as the Persian Gulf and Gulf of California (Figure 1c; Raymond et al., 2020).

The Persian Gulf and Pakistan have the highest ME, and we therefore devote the most space to describing processes there, while also considering other regions in cases where there are notable differences. Extreme-ME composites for both the Persian Gulf and Pakistan reveal a clear influence of moisture advection (Figures 2a and 2c). Over Persian Gulf water, hot and dry northwesterly "shamal" winds efficiently evaporate moisture from the high-SST surface (Xue & Eltahir, 2015), causing the ME and MSE of near-surface air to progressively increase with fetch length, then fall off after encountering desert (Figures 2a and 2b; Figure S3 in Supporting Information S1). Throughout, the mid-troposphere sees only a modest MSE change. In contrast, Pakistan exhibits increasing near-surface ME as the strong onshore flow of the South Asian summer monsoon ascends from the Arabian Sea (Figure 2c), passing over a hot and often irrigated land surface (de Kok et al., 2020). Associated with Pakistan's higher planetary-boundary-layer (PBL) heights, the lower troposphere is much moister overall than in the Persian Gulf. The regions have in common upper-tropospheric subsidence and mid-to-upper-tropospheric dryness, which limit deep moist convection despite moderate-to-high convective available potential energy (Rodwell & Hoskins, 1996; Ziv et al., 2004). They also share apparent damming of the highest ME values against topography, perhaps driven by convergence associated with slowing moisture-laden surface winds (Figure 2).

A more detailed picture of regional processes is provided by time series centered on extreme-ME days (Figure 3). In all regions, anomalous heat and moisture tend to increase and then decrease over the span of several days. Extreme ME is characterized by lower-than-normal (<50th percentile) daytime PBL heights for the Persian Gulf coastline (Figures 3e–3h), but positive PBL-height anomalies at night, likely due to marine moisture limiting surface longwave cooling (Figure 3a). The opposite pattern—anomalously high daytime heights but low nighttime ones—exists on extreme-ME days for eastern South Asia and the western Amazon. Strong diurnal patterns of sensible-heat-flux anomalies in each region help explain the contrasting situations: negative daytime anomalies indicate an anomalously cool land surface in Pakistan and the Persian Gulf, while positive daytime anomalies in eastern South Asia and the western Amazon are consistent with enhanced sensible and latent turbulent heat exchange, driven by a hot land surface and high winds (Figures S4 and S5 in Supporting Information S1). In

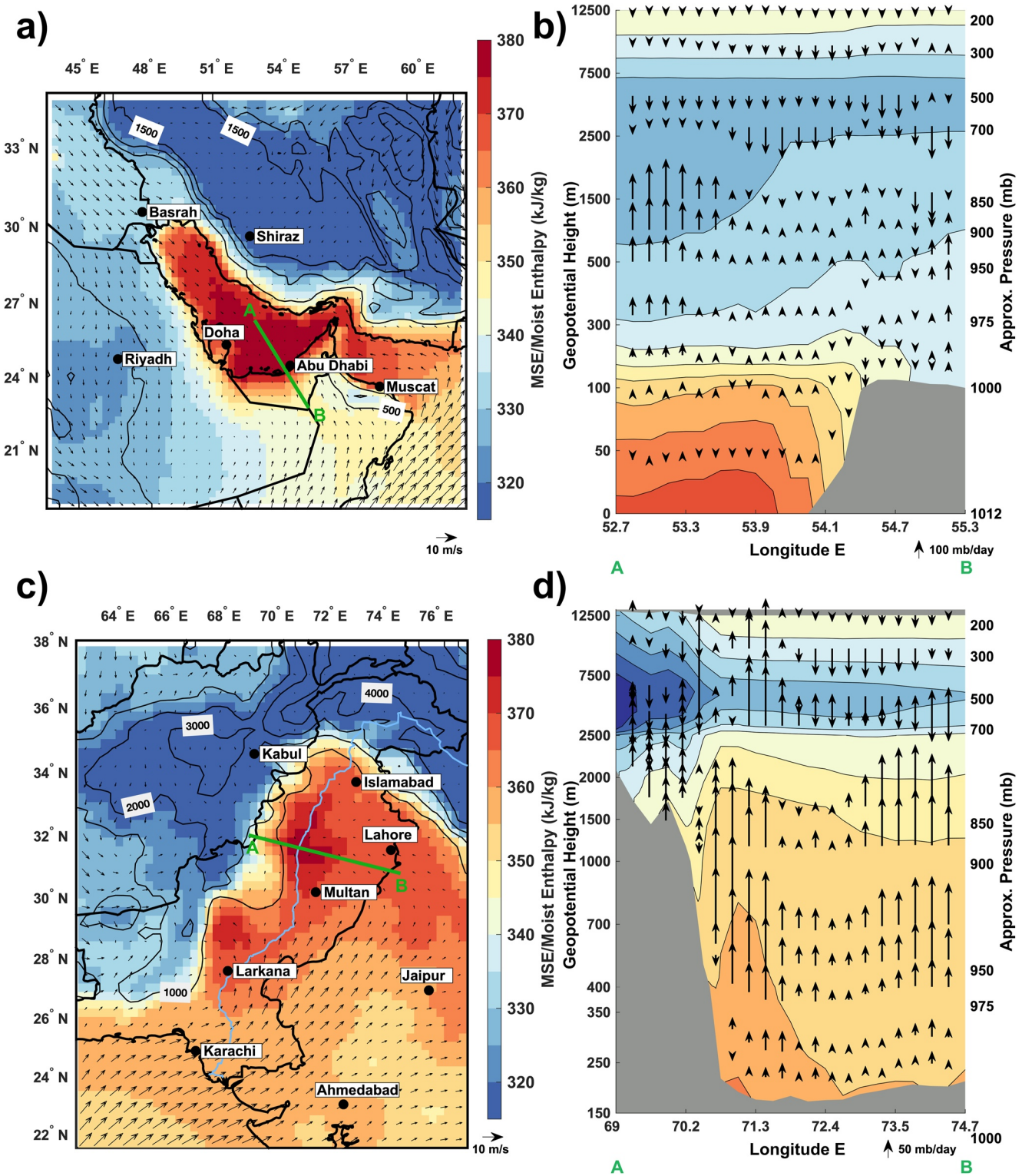

Figure 2. Composite maps of regional extreme-ME days. (a), (c) Composites of 10-m wind and 2-m ME for extreme-ME days in (a) the southern Persian Gulf and (c) north-central Pakistan. Thin black contours mark terrain. Composites are over 163 days in (a) and 109 days in (c). (b), (d) Vertical profile on model-native levels along the cross-sections shown as green lines in (a), (c), with arrows representing vertical velocity, gray shading representing terrain, and colored contours representing MSE according to the same color scheme.

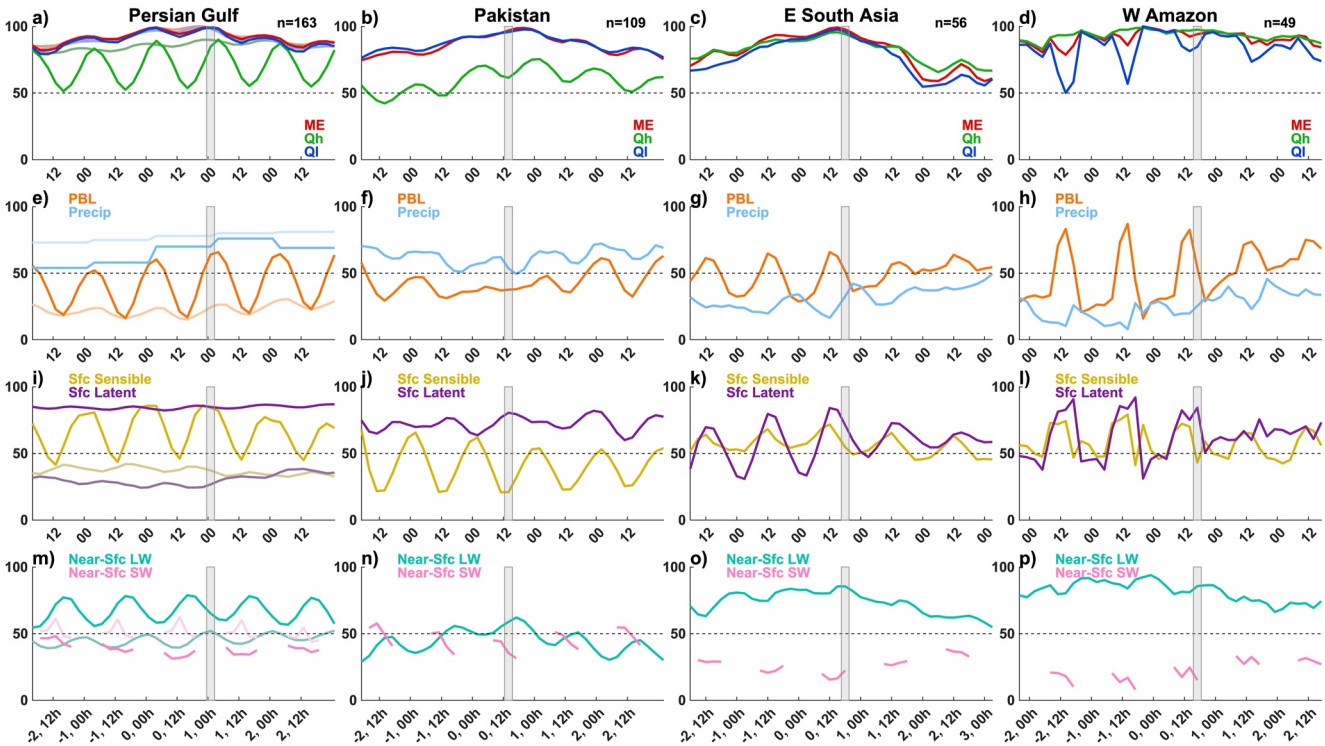

Figure 3. Time series for hotspot regions. Composites surrounding each regional extreme-ME day, for all grid cells exceeding the global 99th percentile and calculated as centiles against the warm-season ME distribution. Dotted lines mark the median (50th percentile). Gray bars indicate the mean time of actual maximum ME. For the Persian Gulf region, grid cells that are more than 50% water are represented by pale lines; elsewhere, they are excluded. Times (00h and 12h) are local standard time. Sample sizes (number of days) are given in the top row, upper right. (a–d) 2-m moist enthalpy, sensible heat, and latent heat. (e–h) Planetary-boundary-layer height and precipitation. (i–l) Surface sensible and latent heat flux. (m–p) Temperature tendency due to 100-m longwave radiation and 100-m shortwave radiation. All fluxes are defined positive toward the 2-m level.

generally hotter and drier Pakistan, extreme-ME days have extreme moisture but moderate temperatures (Figure S6 in Supporting Information S1), while generally higher-humidity eastern South Asia and the western Amazon see extreme-ME days primarily driven by factors that support higher temperatures. However, positive latent-heat-flux anomalies are present in all regions. These processes characterizing ME accumulation have diverse upstream drivers, such as circulation regimes or antecedent soil conditions, worthy of investigation themselves but beyond our scope here.

In sum, we observe that globally extreme ME typically co-occurs with high boundary-layer moisture and an absence of deep convection, and in areas that experience high temperatures. Consequently, we explore whether a simple combination of metrics related to these factors or their drivers might be capable of describing humid-heat hotspots with some accuracy, while recognizing that an explanation of the full global distribution of ME likely involves a much wider array of considerations. In Figure 4, we construct a proxy-based 'prediction' by overlaying measures of high net shortwave and longwave radiation; subsidence; and large moisture availability from either warm SSTs or large latent-heat fluxes. Crucially, these factors include no requirements about the temperature or quantity of moisture near the surface, nor do they presuppose particular meteorological conditions. The overlay closely resembles the actual geographic pattern of Figure 1c (reproduced in Figure 4b), indicating that together they capture well the necessary conditions for globally extreme humid heat.

4. Discussion and Conclusions

We find that the occurrence of the globally highest ME in the subtropics, as identified previously, is most directly a result of (a) strong latent-heat fluxes or advection occurring (b) in the absence of deep convection. Otherwise stated, in all hotspot regions, boundary-layer water vapor accumulates to high concentrations without a mechanism to disperse it into the free troposphere. Such a mechanism may originate from meteorological

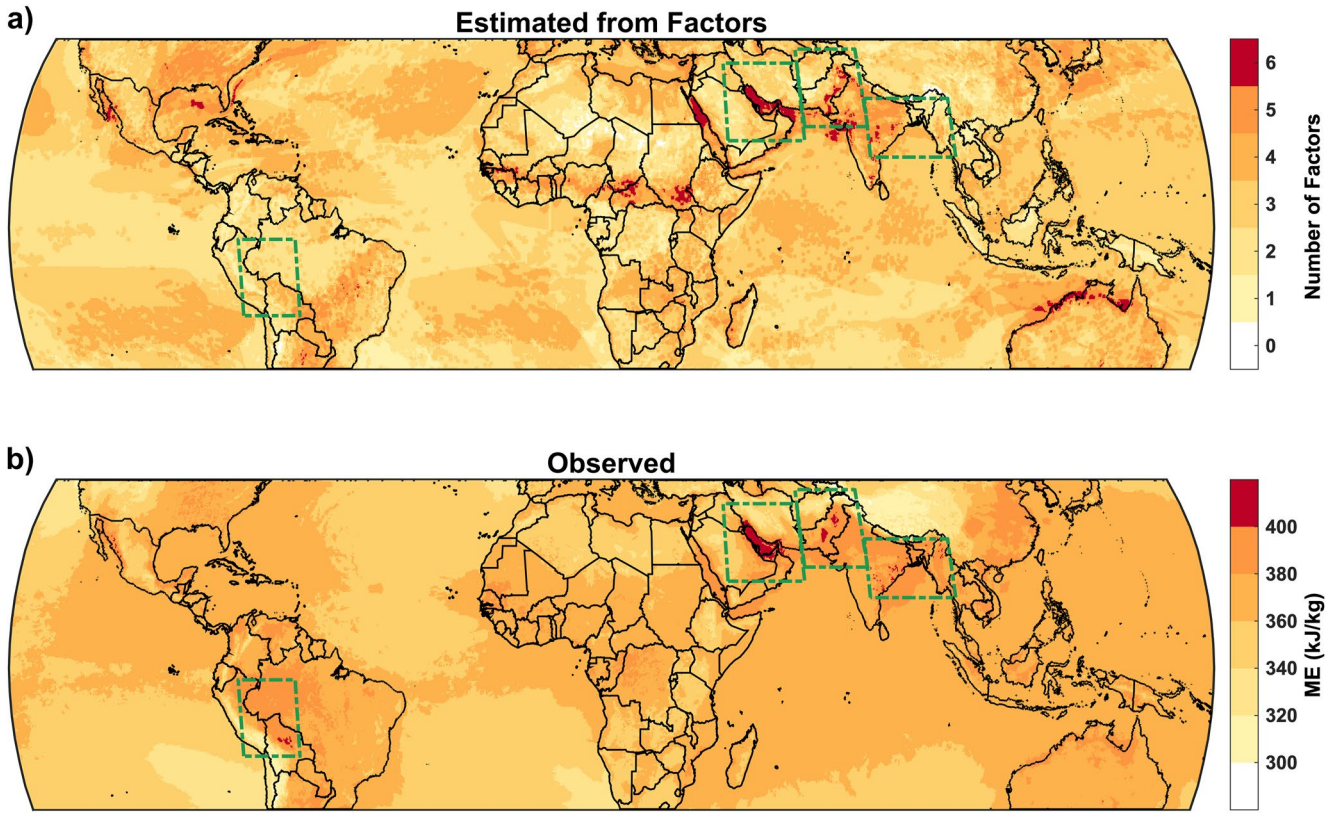

Figure 4. Empirical factors determining the geography of extreme moist enthalpy. (a) Of the factors hypothesized to be important for extreme ME, the number present at each grid cell, assessed via fulfillment of the following criteria: mean warm-season SST >29C within 2 days upwind or median latent-heat flux in the global top 20% of points; median warm-season 850-mb and 300-mb vertical pressure velocity >0; 99th percentile of net shortwave radiation not in the global lowest 10% or highest 10% of points; 99th percentile of net longwave radiation in the global highest 20% of points, but not the highest 10%; annual-median relative humidity between 25% and 75%; and elevation <500 m. (b) Observed all-time maxima of ME, as in Figure 1c.

(i.e., upper-level convergence) or topographical forcing. A dry subtropical mid-troposphere aids in achieving the necessary conditions, as do other factors—including terrain blocking, high nearby SSTs, and low PBL heights—whose relative importances vary by region. For regions with relatively high humid-heat values that we have not focused on, such as eastern China or West Africa, similarity of climate with one of the hotspot regions may serve as a first-order estimate of major controls on high-end humid heat there.

Our results indicate that fully understanding the global patterns of Figure 1c requires considering multiple factors simultaneously; for example, the eastern Mediterranean experiences stronger subsidence than the Persian Gulf, while the Midwest US experiences regional-scale moisture advection, yet neither region sees globally extreme ME (Figure 1; Raymond et al., 2017; Rodwell & Hoskins, 1996). The remainder of the discussion explores in more detail the modes of action of key factors in the hotspot regions, and their implications for extreme-humid-heat location and timing.

The critical role of low-level moisture is highlighted by latent heat being above the 90th percentile during extreme-ME events in all four hotspot regions (Figures 3a–3d). This moisture can originate primarily as evaporation (Xue & Eltahir, 2015), or have a substantial contribution from evapotranspiration (Acosta & Huber, 2020; Drumond et al., 2014). Over Persian Gulf water, high SSTs, high air temperatures, and intense shortwave radiation lead to globally extreme latent heat (Nori et al., 2019; Pal and Eltahir, 2016; Raymond et al., 2020). Low PBL heights—often <200 m—indicate and accentuate trapping of moisture near the surface, creating a large vertical ME gradient (Figures 2b and S3 in Supporting Information S1; Plant & Atkinson, 2002) only partly captured by coarser-resolution cross-sections (Tyrlis et al., 2013). This marine signature is observed over land when the air mass traverses the coastline (Figure 2b; Brooks & Rogers, 2000; Von Engeln & Teixeira, 2013), undergoing heating due to the warm land surface and thereby achieving ME extremes even late in the evening

(Figure 3). However, continued surface heating increases buoyancy, deepening the PBL and mixing in drier air aloft; combined with minimal evaporation from land, near-surface latent heat content then declines (Figure 2b). In Pakistan, latent-heat content is already high at the coast due to monsoonal marine-air advection (Monteiro & Caballero, 2019) but increases further over land, aided by irrigation (Mishra et al., 2020). Indeed, the highest ME closely tracks the Indus Valley's irrigated areas (Figure 2b; de Kok et al., 2020). Under imposed vertical stability due to deep moist convection elsewhere, a decrease in land-surface temperatures shallows the boundary layer, concentrating the effects of surface fluxes and increasing the probability that near-surface air parcels fail to reach the level of free convection—allowing ME to build, independent of ambient vertical stability (Im et al., 2014; Mishra et al., 2020; Krakauer et al., 2020). Eastern South Asia and the western Amazon both also see high latent-heat fluxes (Figure 3k-l), accompanied by cloudiness but high temperatures and low precipitation. In these thickly vegetated regions, such conditions are consistent with high evapotranspiration stemming from large vapor-pressure deficits (Fang et al., 2021). A local pause in deep moist convection may allow for the boundary-layer moisture "reservoirs" to refill (Findell & Eltahir, 2003; Igel, 2017).

Vertical stability—indicated by subsidence, or the general absence of deep moist convection—appears necessary for globally extreme ME. In the tropics, and over tropical oceans specifically, the troposphere is chronically conditionally unstable and consequently sensitive to boundary-layer ME increases (Williams & Renno, 1993; Zhang et al., 2021). Elsewhere, local ME increases lead to convection only when other forcings are conducive. A dry free troposphere (enhanced by subsidence) strongly inhibits convection (Im et al., 2014; Lo & Famiglietti, 2013), as does forced descent by large-scale circulations related to summer monsoons or the Hadley Circulation (Rodwell & Hoskins, 1996; Tromeur & Rossow, 2010; Tyrlis et al., 2013).

Many extreme-ME days feature a lack of precipitation, especially in climatologically more-humid regions such as eastern South Asia and the western Amazon. In the former, high-surface-pressure monsoon-break days are often accompanied by onshore winds, suggesting that regional forcings may simultaneously drive the moisture advection and convection suppression (Krishnan et al., 2009). The resultant instability then causes an uptick in precipitation; this sequence is observed also in the West Pacific, modulated by the Madden-Julian Oscillation (Figures 3g and 3h; Kiranmayi & Maloney, 2011).

In all four hotspot regions, topography guides winds and promotes (or inhibits) vertical mixing, further affecting the locations of extreme ME. Both Pakistan and eastern South Asia see long-distance monsoon-related moisture transport (Krishnan et al., 2009; Acosta & Huber, 2020) which is strengthened and channeled by various mountain ranges and the Tibetan Plateau (Figure 2b; Bollasina & Nigam, 2011; Acosta & Huber, 2017). Similarly, the Iranian Plateau induces subsidence and inhibits westerly advection of lower-ME air (Acosta & Huber, 2020; Zaitchik et al., 2007), favoring build-up of near-surface ME in Pakistan and northern India. The Persian Gulf's shamal winds and sea-breeze circulation are also influenced by topography (Eager et al., 2008; Giannakopoulou & Toumi, 2012; Zhu & Atkinson, 2004) as well as land–sea temperature contrasts (Eager et al., 2008). When regional forcings are weak (Figure S7 in Supporting Information S1; Plant & Atkinson, 2002), the typical nighttime katabatic offshore flow in the southern Persian Gulf (Eager et al., 2008) is replaced by a nearly constant sea breeze (Figure S8 in Supporting Information S1). Complementing these regional-scale observations, we find ME hotspots on the windward side of even small (<1000-m high) topographic features (Figures 2b and 2d; Figure S9 in Supporting Information S1). We hypothesize that these represent pools of relatively stagnant air below elevated topography, such that surface fluxes accumulate while vertical mixing is suppressed; air crossing the barrier experiences forced vertical mixing that moderately decreases near-surface ME on the leeward side (Figure S9 in Supporting Information S1).

The empirical factors we find correlated with globally extreme ME (Figure 4) assist in understanding its general absence from the tropics, despite high tropical median ME (Figure 1). Of particular importance appears to be deep moist convection, echoing dynamical arguments based on tropospheric vertical profiles as well as boundary-layer studies (Gentine et al., 2013; Zhang et al., 2021). Due to conditional instability and tight spatial linkages, the tropical free troposphere-PBL difference in ME—approximately, the boundary-layer capping strength—relates to the temperature difference between the warmest tropical SSTs and the mean (Fueglistaler, 2019), and largely controls tropical extreme-ME magnitude (Larson & Hartmann, 2003; Zhang & Fueglistaler, 2020). The lack of ME hotspots in the tropics can therefore be understood as high ME being translated into convection and effaced on subdaily timescales (Schulz & Stevens, 2018). Studies examining the interface of, and overlap between,

"tropical" and "subtropical" regimes are needed to more fully understand the relevant processes; for example, by regionally assessing the extent to which humid heat is modulated by circulation extremes versus surface fluxes.

A caveat to our results is that biases in ERA5 land-surface schemes, and incomplete representations of topographical effects and ocean dynamics, might mischaracterize the precise magnitude, timing, and location of surface fluxes and advective transport. Temporal and spatial discretization of the data may add to the oversight of brief and localized processes. These weaknesses are shared with other reanalysis-based studies (Donat et al., 2017; Fischer & Knutti, 2013). Considering global patterns, however, even lower-resolution climate models are capable of highlighting the same hotspot regions as in reanalyses (Figure 1c; Suarez-Gutierrez et al., 2020) and station-based assessments (Raymond et al., 2020).

Increasing humid-heat extremes are a critical climate hazard of the twenty-first century. Our study endeavors to develop an empirical process-informed theory for understanding the location and magnitude of global hotspots. We find that these are determined by several factors in conjunction—chief among them a strong supply of water vapor and a lack of substantive boundary-layer mixing. Each condition can emerge through one of several distinct processes: the first through proximity to open water or a land surface moistened from precipitation or irrigation, the second through subsidence from high-pressure systems or local katabatic flow. This complexity showcases the importance of interactions of local and non-local processes, and of geographic and meteorological forcings, against the backdrop of increasing moisture driven by climate warming. Through broadly identifying a hierarchy of critical factors, our study provides a basis for further detailed studies, and for evaluating and efficiently improving models to be capable of better predictions on both weather and climate timescales. Additional regional-modeling experiments interrogating processes and their interactions will be crucial, as will continued reanalysis-product development, while large model ensembles will facilitate refinement of statistics of key variables and their drivers. Such a varied toolkit is essential for better understanding and predicting future humid-heat extremes.

Data Availability Statement

ERA5 data can be downloaded through Copernicus, https://cds.climate.copernicus.eu. NOAA OISST data is found at https://www.ncdc.noaa.gov/oisst, and CHIRPS data at https://www.chc.ucsb.edu/data/chirps. Scripts used to produce the analysis, and the resultant processed datasets, have been archived at https://doi.org/10.5281/zenodo.5095697.

Acknowledgments
A portion of this work was carried out at the Jet Propulsion Laboratory, California Institute of Technology, under a contract with the National Aeronautics and Space Administration (80NM0018D0004).

References

Acosta, R. P., & Huber, M. (2017). The neglected Indo-Gangetic Plains low-level jet and its importance for moisture transport and precipitation during the peak summer monsoon. *Geophysical Research Letters*, *44*, 8601–8610. https://doi.org/10.1002/2017gl074440

Acosta, R. P., & Huber, M. (2020). Competing topographic mechanisms for the Summer Indo-Asian Monsoon. *Geophysical Research Letters*, *47*, e2019gl085112. https://doi.org/10.1029/2019gl085112

Bollasina, M., & Nigam, S. (2011). The summertime "heat" low over Pakistan/northwestern India: Evolution and origin. *Climate Dynamics*, *37*, 957–970. https://doi.org/10.1007/s00382-010-0879-y

Brooks, I. M., & Rogers, D. P. (2000). Aircraft observations of the mean and turbulent structure of a shallow boundary layer over the Persian Gulf. *Boundary-Layer Meteorology*, *95*, 189–210. https://doi.org/10.1029/2000gl012751

Bui, H. X., Yu, J.-Y., & Chou, C. (2016). Impacts of vertical structure of large-scale vertical motion in tropical climate: Moist static energy framework. *Journal of the Atmospheric Sciences*, *73*, 4427–4437. https://doi.org/10.1175/jas-d-16-0031.1

Buzan, J. R., & Huber, M. (2020). Moist heat stress on a hotter Earth. *Annual Review of Earth and Planetary Sciences*, *48*, 623–655. https://doi.org/10.1146/annurev-earth-053018-060100

Chen, X., Li, N., Liu, J., Zhang, Z., Liu, Y., & Huang, C. (2020). Changes in global and regional characteristics of heat stress waves in the 21st century. *Earth's Future*, *8*, e2020ef001636. https://doi.org/10.1029/2020ef001636

Coffel, E. D., Horton, R. M., Winter, J. M., & Mankin, J. S. (2019). Nonlinear increases in extreme temperatures paradoxically dampen increases in extreme humid-heat. *Environmental Research Letters*, *14*, 084003. https://doi.org/10.1088/1748-9326/ab28b7

De Kok, R. J., Kraaijenbrink, P. D. A., Tuinenburg, O. A., Bonekamp, P. N. J., & Immerzeel, W. W. (2020). Towards understanding the pattern of glacier mass balances in High Mountain Asia using regional climatic modelling. *The Cryosphere*, *14*, 3215–3234. https://doi.org/10.5194/tc-14-3215-2020

Donat, M. G., Pitman, A. J., & Seneviratne, S. I. (2017). Regional warming of hot extremes accelerated by surface energy fluxes. *Geophysical Research Letters*, *44*, 7011–7019. https://doi.org/10.1002/2017gl073733

Drumond, A., Marengo, J., Ambrizzi, T., Nieto, R., Moreira, L., & Gimeno, L. (2014). The role of the Amazon Basin moisture in the atmospheric branch of the hydrological cycle: A Lagrangian analysis. *Hydrology and Earth System Sciences*, *18*, 2577–2598. https://doi.org/10.5194/hess-18-2577-2014

Dunne, J. P., Stouffer, R. J., & John, J. G. (2013). Reductions in labour capacity from heat stress under climate warming. *Nature Climate Change*, *3*, 563–566. https://doi.org/10.1038/nclimate1827

Eager, R. E., Raman, S., Wootten, A., Westphal, D. L., Reid, J. S., & Al Mandoos, A. (2008). A climatological study of the sea and land breezes in the Arabian Gulf region. *Journal of Geophysical Research*, *113*, d15106. https://doi.org/10.1029/2007jd009710

Eltahir, E. A. B., & Pal, J. S. (1996). Relationship between surface conditions and subsequent rainfall in convective storms. *Journal of Geophysical Research*, *101*(D21), 26237–26245. https://doi.org/10.1029/96jd01380

Fallah, A., Rakhshandehroo, G. R., Berg, P., O, S., & Orth, R. (2020). Evaluation of precipitation datasets against local observations in southwestern Iran. *International Journal of Climatology*, *40*(9), 4102–4116. https://doi.org/10.1002/joc.6445

Fang, Y., Leung, L. R., Wolfe, B. T., Detto, M., Knox, R., McDowell, N., et al. (2021). Disentangling the effects of vapor pressure deficit and soil water availability on canopy conductance in a seasonal tropical forest during the 2015 El Niño drought. *Journal of Geophysical Research - D: Atmospheres*, *126*(10), e2021jd035004. https://doi.org/10.1029/2021jd035004

Findell, K. L., & Eltahir, E. A. B. (2003). Atmospheric controls on soil moisture-boundary layer interactions. Part II: Feedbacks within the continental United States. *Journal of Hydrometeorology*, *4*, 5702–6583. https://doi.org/10.1175/1525-7541(2003)004<0570:acosml>2.0.co;2

Fischer, E. M., & Knutti, R. (2013). Robust projections of combined humidity and temperature extremes. *Nature Climate Change*, *3*, 126–130. https://doi.org/10.1038/nclimate1682

Freychet, N., Tett, S. F. B., Yan, Z., & Li, Z. (2020). Underestimated change of wet-bulb temperatures over East and South China. *Geophysical Research Letters*, *47*, e2019gl086140. https://doi.org/10.1029/2019gl086140

Fueglistaler, S. (2019). Observational evidence for two modes of coupling between sea surface temperatures, tropospheric temperature profile, and shortwave cloud radiative effect in the tropics. *Geophysical Research Letters*, *46*, 9890–9898. https://doi.org/10.1029/2019gl083990

Funk, C., Peterson, P., Landsfeld, M., Pedreros, D., Verdin, J., Shukla, S., et al. (2015). The climate hazards infrared precipitation with stations – A new environmental record for monitoring extremes. *Scientific Data*, *2*(1), 150066. https://doi.org/10.1038/sdata.2015.66

Gentine, P., Holtslag, A. A. M., D'Andrea, F., & Ek, M. (2013). Surface and atmospheric controls on the onset of moist convection over land. *Journal of Hydrometeorology*, *14*, 443–462. https://doi.org/10.1175/jhm-d-12-0137.1.c.

Giannakopoulou, E. M., & Toumi, R. (2012). The Persian Gulf summertime low-level jet over sloping terrain. *The Quarterly Journal of the Royal Meteorological Society*, *138*, 145–157. https://doi.org/10.1002/qj.901

Hanna, E. G., & Tait, P. W. (2015). Limitations to thermoregulation and acclimatization challenge human adaptation to global warming. *International Journal of Environmental Research and Public Health*, *12*, 8034–8074. https://doi.org/10.3390/ijerph120708034

Hersbach, H., Bell, B., Berrisford, P., Hirahara, S., Horányi, A., Muñoz-Sabater, J., et al. (2020). The ERA5 global reanalysis. *The Quarterly Journal of the Royal Meteorological Society*, *146*, 1999–2049. https://doi.org/10.1002/qj.3803

Huang, J. (2018). A simple accurate formula for calculating saturation vapor pressure of water and ice. *Journal of Applied Meteorology and Climatology*, *57*, 1265–1272. https://doi.org/10.1175/jamc-d-17-0334.1

Igel, M. R. (2017). The tropical precipitation pickup threshold and clouds in a radiative convective equilibrium model: 2. Two-layer moisture. *Journal of Geophysical Research - D: Atmospheres*, *122*, 6469–6487. https://doi.org/10.1002/2016jd025908

Im, E.-S., Kang, S., & Eltahir, E. A. B. (2018). Projections of rising heat stress over the western Maritime Continent from dynamically downscaled climate simulations. *Global and Planetary Change*, *165*, 160–172. https://doi.org/10.1016/j.gloplacha.2018.02.014

Im, E.-S., Marcella, M. P., & Eltahir, E. A. B. (2014). Impact of potential large-scale irrigation on the West African Monsoon and its dependence on location of irrigated area. *Journal of Climate*, *27*, 994–1009. https://doi.org/10.1175/jcli-d-13-00290.1

Im, E.-S., Pal, J. S., & Eltahir, E. A. B. (2017). Deadly heat waves projected in the densely populated agricultural regions of South Asia. *Science Advances*, *3*, e1603322. https://doi.org/10.1126/sciadv.1603322

Kenney, W. L., DeGroot, D. W., & Holowatz, L. A. (2004). Extremes of human heat tolerance: Life at the precipice of thermoregulatory failure. *Journal of Thermal Biology*, *29*, 479–485. https://doi.org/10.1016/j.jtherbio.2004.08.017

Kiranmayi, L., & Maloney, E. D. (2011). Intraseasonal moist static energy budget in reanalysis data. *Journal of Geophysical Research*, *116*, D21117. https://doi.org/10.1029/2011jd016031

Krakauer, N. Y., Cook, B. I., & Puma, M. J. (2020). Effect of irrigation on humid heat extremes. *Environmental Research Letters*, *15*, 094010. https://doi.org/10.1088/1748-9326/ab9ecf

Krishnan, R., Kumar, V., Sugi, M., & Yoshimura, J. (2009). Internal feedbacks from monsoon-midlatitude interactions during droughts in the Indian Summer Monsoon. *Journal of the Atmospheric Sciences*, *66*, 553–578. https://doi.org/10.1175/2008jas2723.1

Larson, K., & Hartmann, D. L. (2003). Interactions among cloud, water vapor, radiation, and large-scale circulation in the tropical climate. Part I: Sensitivity to uniform sea surface temperature changes. *Journal of Climate*, *16*, 1425–1440. https://doi.org/10.1175/1520-0442-16.10.1425

Li, D., Yuan, J., & Kopp, R. E. (2020). Escalating global exposure to compound heat-humidity extremes with warming. *Environmental Research Letters*, *15*, 064003. https://doi.org/10.1088/1748-9326/ab7d04

Lo, M.-H., & Famiglietti, J. S. (2013). Irrigation in California's Central Valley strengthens the southwestern U.S. water cycle. *Geophysical Research Letters*, *40*, 301–306. https://doi.org/10.1002/grl.50108

Lutsko, N. J. (2021). The relative contributions of temperature and moisture to heat stress changes under warming. *Journal of Climate*, *34*, 901–917. https://doi.org/10.1175/jcli-d-20-0262.1

Matthews, T. (2018). Humid heat and climate change. *Progress in Physical Geography*, *42*(3), 391–405. https://doi.org/10.1177/0309133318776490

Mishra, V., Ambika, A. K., Asoka, A., Aadhar, S., Buzan, J., Kumar, R., & Huber, M. (2020). Moist heat stress extremes in India enhanced by irrigation. *Nature Geoscience*, *13*, 722–728. https://doi.org/10.1038/s41561-020-00650-8

Monteiro, J. M., & Caballero, R. (2019). Characterization of extreme wet-bulb temperature events in southern Pakistan. *Geophysical Research Letters*, *46*, 10659–10668. https://doi.org/10.1029/2019gl084711

Mora, C., Dousset, B., Caldwell, I. R., Powell, F. E., Geronimo, R. C., Bielecki, C. R., et al. (2017). Global risk of deadly heat. *Nature Climate Change*, *7*, 501–506. https://doi.org/10.1038/nclimate3322

Noori, R., Tian, F., Berndtsson, R., Abbasi, M. R., Naseh, M. V., Modabberi, A., et al. (2019). Present and future trends in sea surface temperature across the Persian Gulf and Gulf of Oman. *PLoS One*, *14*, e0212790. https://doi.org/10.1371/journal.pone.0212790

Pal, J. S., & Eltahir, E. A. B. (2016). Future temperature in southwest Asia projected to exceed a threshold for human adaptability. *Nature Climate Change*, *6*. https://doi.org/10.1038/nclimate2833

Plant, R. S., & Atkinson, B. W. (2002). Sea-breeze modification of the growth of a marine internal boundary layer. *Boundary-Layer Meteorology*, *104*, 201–228. https://doi.org/10.1023/a:1016045229957

Raymond, C., Matthews, T., & Horton, R. M. (2020). The emergence of heat and humidity too severe for human tolerance. *Science Advances*, *6*, 19. https://doi.org/10.1126/sciadv.aaw1838

Raymond, C., Singh, D., & Horton, R. M. (2017). Spatiotemporal patterns and synoptics of extreme wet-bulb temperature in the contiguous United States. *Journal of Geophysical Research - D: Atmospheres*, *122*, 108–113. https://doi.org/10.1002/2017jd027140

Reynolds, R. W., Rayner, N. A., Smith, T. M., Stokes, D. C., & Wang, W. (2002). An improved in situ and satellite SST analysis for climate. *Journal of Climate*, *15*, 16092–21625. https://doi.org/10.1175/1520-0442(2002)015<1609:aiisas>2.0.co;2

Rodwell, M. J., & Hoskins, B. J. (1996). Monsoons and the dynamics of deserts. *Quarterly Journal of the Royal Meteorological Society*, *122*, 1385–1404. https://doi.org/10.1002/qj.49712253408

Schulz, H., & Stevens, B. (2018). Observing the tropical atmosphere in moisture space. *Journal of the Atmospheric Sciences*, *75*, 3313–3330. https://doi.org/10.1175/jas-d-17-0375.1

Sherwood, S. C., & Huber, M. (2010). An adaptability limit to climate change due to heat stress. *Proceedings of National Academy of Sciences of the USA*, *107*, 9552–9555. https://doi.org/10.1073/pnas.0913352107

Suarez-Gutierrez, L., Müller, W. A., Li, C., & Marotzke, J. (2020). Hotspots of extreme heat under global warming. *Climate Dynamics*, *55*, 429–447. https://doi.org/10.1007/s00382-020-05263-w

Tromeur, E., & Rossow, W. B. (2010). Interaction of tropical deep convection with the large-scale circulation in the MJO. *Journal of Climate*, *23*(7), 1837–1853. https://doi.org/10.1175/2009jcli3240.1

Tyrlis, E., Lelieveld, J., & Steil, B. (2013). The summer circulation over the eastern Mediterranean and the Middle East: Influence of the South Asian monsoon. *Climate Dynamics*, *40*, 1103–1123. https://doi.org/10.1007/s00382-012-1528-4

Von Engeln, A., & Teixeira, J. (2013). A planetary boundary layer height climatology derived from ECMWF reanalysis data. *Journal of Climate*, *26*, 6575–6590. https://doi.org/10.1175/jcli-d-12-00385.1

Willett, K. M., & Sherwood, S. (2012). Exceedance of heat index thresholds for 15 regions under a warming climate using the wet-bulb globe temperature. *International Journal of Climatology*, *32*, 161–177. https://doi.org/10.1002/joc.2257

Williams, E., & Renno, N. (1993). An analysis of the conditional instability of the tropical atmosphere. *Monthly Weather Review*, *121*, 21–36. https://doi.org/10.1175/1520-0493(1993)121<0021:aaotci>2.0.co;2

Xue, P., & Eltahir, E. A. B. (2015). Estimation of the heat and water budgets of the Persian (Arabian) Gulf using a regional climate model. *Journal of Climate*, *28*, 5041–5062. https://doi.org/10.1175/jcli-d-14-00189.1

Zaitchik, B. F., Evans, J. P., & Smith, R. B. (2007). Regional impact of an elevated heat source: The Zagros Plateau of Iran. *Journal of Climate*, *20*, 4133–4146. https://doi.org/10.1175/jcli4248.1

Zhang, Y., & Fueglistaler, S. (2020). How tropical convection couples high moist static energy over land and ocean. *Geophysical Research Letters*, *47*. https://doi.org/10.1029/2019gl086387

Zhang, Y., Held, I., & Fueglistaler, S. (2021). Projections of tropical heat stress constrained by atmospheric dynamics. *Nature Geoscience*, *14*, 133–137. https://doi.org/10.1038/s41561-021-00695-3

Zhu, M., & Atkinson, B. W. (2004). Observed and modelled climatology of the land-sea breeze circulation over the Persian Gulf. *International Journal of Climatology*, *24*, 883–905. https://doi.org/10.1002/joc.1045

Ziv, B., Saaroni, H., & Alpert, P. (2004). The factors governing the summer regime of the eastern Mediterranean. *International Journal of Climatology*, *24*, 1859–1871. https://doi.org/10.1002/joc.1113